Endometriotic Organoids: A Novel In Vitro Model of Endometriotic Lesion Development.

Yong Song[1†], Gregory W. Burns[1†], Niraj R. Joshi[1], Ripla Arora[1], J. Julie Kim[2] and Asgerally T. Fazleabas[1*]

[1]Department of Obstetrics, Gynecology and Reproductive Biology, Michigan State University, Grand Rapids, MI 49503, USA

[2]Department of Obstetrics and Gynecology, Feinberg School of Medicine, Northwestern University, Chicago, IL, USA

[†]These authors contributed equally.

*Corresponding author. Email: fazleaba@msu.edu

One Sentence Summary:

Endometriotic organoids are an appropriate model to study epithelial-stromal interactions and model cell invasion associated with lesion development.

ABSTRACT

The development and progression of endometriotic lesions are poorly understood, but immune cell dysfunction and inflammation are closely associated with the pathophysiology of endometriosis. A lack of suitable 3D *in vitro* models permitting the study of interactions between cell types and the microenvironment is a contributing factor. To address this limitation, we developed endometriotic organoids (EO) to explore the role of epithelial-stromal interactions and model peritoneal cell invasion associated with lesion development. Using a non-adherent microwell culture system, spherical organoids were generated with endometriotic epithelial cells (12Z) combined with immortalized endometriotic stromal cells (iEc-ESC) or immortalized uterine stromal cells (iHUF). Organoids self-organized with stromal cells occupying the center and epithelial cells on the periphery of the organoid. Endometriotic organoids (EO), containing iEc-ESC, resulted in the development of stratified 12Z epithelial cells compared to those with iHUF where the 12Z cells developed as a single layered epithelium. Transcriptomic analysis found 4,522 differentially expressed genes (DEG) between EO and 12Z/iHUF organoids, and the top DEG included increased expression of interleukins and prostaglandin synthase enzymes. An overlap of the EO DEG with baboon endometriotic lesions was highly significant. Finally, to mimic invasion of endometrial tissue into the peritoneum, a model was developed using EO and extracellular matrix containing human peritoneal mesothelial cells (LP9). Invasion of EO into the extracellular matrix-LP9 layer was increased in presence of estrogen or THP1-derived proinflammatory macrophages. Taken together, our results strongly support the concept that EO are an appropriate model for dissecting mechanisms that contribute to endometriotic lesion development.

INTRODUCTION

Endometriosis is a chronic inflammatory hormone-dependent disorder which is characterized by the presence of endometrial tissue outside the uterus (*1*). It affects between 10 and 15% of all women of reproductive age, 70% of women with chronic pelvic pain, and 20–50% women with infertility (*2, 3*). An average 7-10 years delay between the onset of symptoms and definitive diagnosis places an enormous emotional and financial burden on both the patient and the healthcare system, with annual costs exceeding $78 billion each year in the United States alone (endofound.org). Quality of life is reduced in women with endometriosis due to painful symptoms, which result in a loss of 11 hours of productivity per week (endofound.org). The etiology and pathogenesis of endometriosis remains unclear, but lesion development has been associated with cellular proliferation and invasion, and interactions between endometriotic cells, immune cells and their microenvironment (*4, 5*). Appropriate *in vitro* platforms that allow dissection of the underlying mechanisms of these processes will inform the understanding of the disease and development of novel therapeutics.

Clinical samples from patients with endometriosis are the first line model to investigate the disease. One of the major limitations to understanding the pathological events associated with endometriosis is the significant delay of 8-11 years for diagnosis and subsequent variations in disease etiology and progression. Thus, both *in vivo* and *in vitro* models are indispensable to study the cellular and molecular mechanisms associated with endometriotic lesion development at different stages, The non-human primate and rodent models of endometriosis have been used most exclusively for *in vivo* studies. Non-human primates offer a physiologically relevant model and provide an opportunity to study both the early events and the disease progression (*6, 7*). Rodent models are advantageous due to the ability for tissue-specific gene manipulation and initial *in vivo* therapeutic testing (*8*). Most *in vitro* studies utilize two-dimensional monolayer culture of primary or immortalized endometrial cells. This method allows for the study of endometriosis associated mechanisms in a cell-specific manner and is easily manipulated for testing of treatments. However, the interactions are limited to the horizontal plane and cells are exposed to

65 a uniform concentration of factors, so monolayer cultures are unable to mimic the architecture
66 and function of tissues *in situ*. Thus, there is a significant gap between *in vivo* models and current
67 *in vitro* cell culture techniques. Three-dimensional (3D) spheroids, or organoids, provide an
68 exciting method to bridge the gap by incorporation of more complex structures and multiple cell
69 types.

70 Organoids are self-organizing, genetically stable, 3D culture systems containing both
71 progenitor/stem and differentiated cells that resemble the tissue of origin (*9-13*). Boretto et al. first
72 established endometriotic epithelial organoids in a Matrigel organoid culture system using ectopic
73 lesions from patients with endometriosis and reported that the organoids replicated disease-
74 associated functional and genomic traits (*14*). This system only allowed for the culture of
75 endometriotic epithelial cells. However, endometrial assembloids containing epithelium and
76 stroma were possible when epithelial organoids were later combined with stromal cells in a
77 collagen hydrogel (*15*). Wiwatpanit et al. generated endometrial organoids containing both
78 epithelial and stromal cells from endometrial biopsies using micro-molded agarose plates and the
79 scaffold-free organoids resembled the physiology of the normal endometrium (*13*). The micro-
80 molded agarose plate organoid culture system is more cost effective, does not require exogenous
81 scaffold materials but relies on *de novo* secretion of extracellular matrix, and allows for self-
82 organization and growth of multiple cell types.

83 An SV40-tranformed endometriotic epithelial cell line derived from peritoneal endometriosis,
84 12Z, is widely used for the study of endometriosis (*16*) and we recently developed an
85 endometriotic stromal cell line (iEc-ESC) from ovarian endometriosis (*17*). In this study, our aim
86 was to develop an endometriotic organoid model containing both endometriotic epithelial and
87 stromal cell lines. We hypothesized that the transcriptome of scaffold-free organoids containing
88 both endometriotic cell types would mirror endometriotic lesions from the baboon model and
89 provide a model to explore peritoneal invasion associated with endometriotic lesion initiation.

90 **RESULTS**

91 **Epithelial and Stromal Cells Self-Organize in Organoids**

92 Epithelial and stromal cells are the two main cell types found in endometriotic lesions that are
93 hypothesized to be descended from retrograde menstrual endometrial fragments. The cells
94 employed in this study were immortalized ectopic epithelial cells (12Z), ectopic stromal cells (iEc-
95 ESC) and human uterine fibroblasts (iHUF) (*16, 17*). For live visualization of cell-type organization,
96 epithelial 12Z cells were modified to express red fluorescent protein (RFP) and both stromal cell
97 lines to express Azurite blue. Endometrial organoids were generated from epithelial 12Z or
98 stromal iEc-ESC alone, 12Z+iHUF, and 12Z+iEc-ESC in micro-molded agarose well plates. A
99 preliminary study empirically determined that the optimal ratio of epithelial cells to stromal cells
100 for co-culture was 1:50. Time-lapse imaging demonstrated that epithelial and stromal cells
101 reorganized autonomously in the agarose wells (Supplemental Video 1). The organization was
102 confirmed by confocal image Z-stack reconstructions and immunohistochemical staining on days
103 4 and 7 (Fig 1). In 12Z+iHUF (Fig 1A) and 12Z+iEc-ESC (EO) (Fig 1B) organoids, epithelial cells
104 were located on the periphery of a stromal cell core by day 4. EO developed multiple epithelial
105 cell layers (Fig 1B), while 12Z+iHUF resulted in a single layer of epithelial cells at day 7 (Fig 1A).
106 Organoids containing only epithelial 12Z or stromal iEc-ESC formed simple spheroid structures
107 (Supplemental Fig 1).

108 **Endometriotic Organoids Invade a 3D Model of the Peritoneum**

109 Cell invasion is one of the key processes involved in endometriotic lesion initiation and
110 development. To simulate cell invasion that occurs *in vivo*, we developed a 3D endometriotic
111 organoid invasion model. As shown in Fig 2A, human peritoneal mesothelial cells, LP9,
112 expressing GFP were grown in Matrigel to mimic the structure of the peritoneum. Endometriotic
113 organoids containing iEc-ESC and 12Z were seeded on the top of the LP9/Matrigel layer. The
114 invasion of organoids was tracked using a fluorescent confocal microscopy every other day for 7
115 days. The Z-stack images were reconstructed to produce 3D models with Imaris image analysis
116 software by Bitplane. As shown in Supplemental Video 2 and Fig 2C, the organoids invaded the
117 Matrigel and continued penetrating the LP9 cell layer. Interestingly, stromal cells were always
118 noted at the leading edge of invasion and as the first cell type to penetrate the LP9 cell layer. The

119 organoid invasion was quantified, and data are shown in Fig 2B. Combined, these results support
120 the idea that the organoid invasion model could be an ideal *in vitro* tool to study the early events
121 of endometriosis, particularly with respect to cell invasion.

122 **Estrogen Stimulates Invasion of Endometriotic Organoids**

123 Endometriosis is estrogen-dependent disease and estrogen can promote the migration and
124 invasion of endometrial stromal cells and endometriotic epithelial cells in two-dimensional culture
125 (*18, 19*). However, the effect of estrogen on organoids is unknown but we hypothesized that
126 estradiol would stimulate invasion in our model. Invasion of Day 4 EO through the Matrigel/LP9
127 cell layer was monitored in the presence of 20nM estradiol (E2) or vehicle for 4 days. Organoids
128 were imaged on Day 1 and Day 4 by fluorescent confocal microscopy. The invasion rate of
129 endometriotic organoids was increased at 1.8-fold in the presence of E2 compared to vehicle
130 ($p<0.05$; Fig 3).

131 **Stromal Cell Origin Alters Organoid Gene Expression**

132 We profiled the transcriptomes by RNA-sequencing of organoids containing ectopic stromal
133 and epithelial cell lines (iEc-ESC/12Z; EO) and compared the profile to normal stromal and ectopic
134 epithelial organoids (iHUF/12Z) to identify the global transcriptomic effect of ectopic stromal cells
135 in the organoids. As an indication of broad transcriptome differences, EO and iHUF/12Z organoid
136 samples were separated by principal component analysis across PC1 (65.7%, Fig 4A) and
137 unsupervised hierarchical clustering (Fig 4B). Indeed, there were 4,522 differentially expressed
138 genes (DEG), with 2,175 increased and 2,347 decreased, in EO compared to iHUF/12Z organoids.
139 The top 50 DEG included increased expression of interleukins (*IL1B*, *IL24*), prostaglandin
140 synthase enzymes (*PTGS1*, *PTGS2*), and telomerase reverse transcriptase (*TERT*). Of note,
141 stromal cell lines were immortalized by constitutive expression of *TERT* via lentiviral transduction,
142 but *TERT* was not differentially expressed in an analysis of organoids containing only stromal
143 cells (Supplemental Fig 2), indicating the altered expression was due to an interaction between
144 the epithelial and stromal cells.

145 Prostaglandin synthase enzymes, *PTGS1* and *PTGS2*, *CXCL8*, *TIMP3*, an inactivator of

146 extracellular matrix remodeling enzymes, *IL1A*, and *LIF*, an estrogen response gene, were
147 increased in EO while *STRA6* and *CRABP2*, retinoic acid binding proteins, and *PGR* were down-
148 regulated (Fig 5A). Gene set enrichment analysis (GSEA) results included NFKB target genes,
149 two senescence gene sets, and TNFα response via p38 mitogen-activated protein kinases as the
150 most highly increased gene sets for EO, while stem cell-associated genes, including *CDKN2C*,
151 *CDH11*, and *ROR1*, were decreased (Fig 5B).

152 **Ectopic Organoids are Similar to Endometriotic Lesions**

153 RNA-sequencing data from baboon endometrium and endometriotic lesions was compared
154 to the human organoids and overlap of gene expression between these comparisons was highly
155 significant, with 12,504 commonly expressed genes (Fig 6A). Additionally, GSEA using hallmark
156 gene sets found similarities for comparisons of EO versus iHUF/12Z organoids and spontaneous
157 baboon ectopic lesions versus eutopic endometrium (Fig 6B). TNF signaling via NFKB,
158 inflammatory responses, and hypoxia associated genes were increased in EO and baboon
159 lesions, while interferon alpha response was decreased in EO and increased in lesions. Similarly,
160 allograft rejection and IL6 JAK/STAT3 signaling gene sets were increased in baboon ectopic
161 lesions compared to eutopic tissues but absent from the organoid comparison. Gene ontology
162 analysis of 2,518 genes identified only as expressed in baboon tissues resulted in significant
163 enrichment for PANTHER GO-slim terms associated with the immune system (Table 1).

164 **Proinflammatory Macrophages Increase Endometriotic Organoid Invasion**

165 Immune cell dysfunction and local inflammation in the endometriotic environment have been
166 considered to play a pivotal role in the pathogenesis of endometriosis (*20*). The recruitment of
167 macrophages within the endometriotic lesion have been demonstrated to facilitate the
168 development and maintenance of endometriosis (*21-23*). In support of a role for macrophages in
169 the pathophysiology of endometriosis, immunoreactive CD68, a pan-macrophage marker, was
170 detected in a baboon endometriotic lesion (Supplemental Fig 3). Proinflammatory, or M1,
171 macrophages have the capacity to secrete inflammatory cytokines, including IL-6. These
172 inflammatory cytokines may further promote endometriotic cell growth and invasion (*24*). To

173 address the effect of activated proinflammatory macrophages on EO invasion, M1 were
174 differentiated from naïve (M0) macrophages derived from the THP1 cell line by exposure to IFN-
175 γ and lipopolysaccharide (LPS) for 24 hours. The resulting proinflammatory macrophages were
176 acclimatized for 24-36 hours in the organoid culture medium. As before, EO added to the top of
177 the Matrigel/LP9 layer and proinflammatory macrophages were added to the wells three hours
178 later. The EO were imaged on days 1 and 3 using fluorescent laser-scanning confocal microscopy.
179 Co-culture with either 7,500 or 15,000 macrophages increased EO invasion by 1.6- or 1.7-fold,
180 respectively, while there was no difference between the macrophage treatment groups (Fig 7).
181 Thus, the addition of proinflammatory macrophages promoted the endometriotic organoid
182 invasion in support of the hypothesis that macrophages facilitate the establishment of
183 endometriotic lesions.

184 **DISCUSSION**

185 A 3D organoid consisting of both epithelial and stromal cells hold promise as an excellent
186 model for dissecting mechanisms associated with early endometriotic lesion development. Most
187 cases of endometriosis are hypothesized to be the result of retrograde menstruation of
188 endometrial fragments containing both epithelium and stroma (*25, 26*). Therefore, inclusion of
189 both cell types more closely resembles the pathophysiology of endometriosis and advances the
190 potential for *in vitro* discovery. Ultra-low attachment plates and hanging drop culture have been
191 used to generate spheroids with 12Z cells, immortalized stromal cells or primary ectopic stromal
192 cells, or a combination of epithelial and stromal cells to investigate endometriosis (*27, 28*).
193 Interestingly, both of these culture models formed self-organizing spheroid structures, but
194 separate epithelial and stromal cell compartments were evident only in ultra-low attachment
195 conditions (*27*); indicating that ultra-low attachment culture might be more suitable for developing
196 organoids with multiple cell types.

197 In this study, we developed EO with endometriotic epithelial and stromal cell lines using a
198 micro-molded agarose plate culture system. Organoids self-organized and resulted in a stromal
199 cell core surrounded by epithelial cells, a morphology is similar to that of endometrial organoids

200 derived from primary endometrial cells (*13*). Interestingly, the origin of the stromal cells, normal or
201 ectopic, altered the organoid structure with stratified epithelial cells forming only with ectopic
202 stromal cells. The observed epithelial stratification is consistent with reports of endometriotic
203 epithelial organoids grown in Matrigel (*14*) and suggests that the ectopic stromal cells promoted
204 epithelial cell proliferation and loss of apical-basal polarity. Transcriptomic analyses revealed that
205 known pathways dysregulated in endometriotic lesions were present in EO, supporting the idea
206 that EO reproduce many hallmarks of the endometriosis-associated transcriptome. Of note,
207 normal endometrial epithelial cell lines were not included in this study and are not currently readily
208 available, although an SV40-transfromed endometrial epithelial cell line, hEM3 was recently
209 reported (*29*). Therefore, some of the gene signatures obtained from the classic comparison of
210 endometriotic lesion versus normal endometrium may be absent from our study due to the
211 limitation that both organoid types included diseased epithelium. This comparison, however,
212 highlighted the effect of stromal cell origin on epithelial phenotype and poses important questions
213 regarding the contribution of each cell compartment to the pathophysiology of lesions. Overall,
214 our results support the idea that EO largely recapitulate the properties of endometriotic lesions
215 with respect to morphology, function, and gene expression.

216 Attachment and invasion are important steps in the development of endometriotic lesions (*4*).
217 Most current methods to study cell invasion are based on single cell types in 2D culture or
218 Transwell assays. We developed a 3D organoid invasion model based on peritoneal
219 endometriotic lesions to more accurately simulate the cell invasion process that occurs *in vivo*. To
220 our knowledge, this is the first 3D invasion model which includes the three main cell compartments,
221 epithelium, stroma and peritoneal mesothelium. Endometriotic organoids migrated through a layer
222 of Matrigel, contacted, and penetrated through a layer of mesothelial cells, to mimic peritoneal
223 invasion. Interestingly, our results identified stromal cells at the leading edge of invasion despite
224 their location at the center of the organoid. This observation agrees with previous studies
225 investigating adhesion and invasion of endometrium to peritoneum using both nude mice and *ex*
226 *vivo* tissue explant culture models (*30, 31*). Endometrial stromal cells from women with

227 endometriosis undergo changes in adhesive properties and mesenchymal characteristics in
228 response to peritoneal mesothelial cells that might be part of the underlying mechanisms of lesion
229 initiation (*32*). Our data indicate that endometriotic organoids have the capacity to invade a
230 monolayer of mesothelial cells in a manner hypothesized to occur in physiological conditions. The
231 utility of this model was further supported by increased invasive capacity in the presence of
232 estrogen or activated proinflammatory macrophages. Collectively, this model expands the
233 possibilities to study mechanisms of endometriotic lesion establishment *in vitro*.

234 Stromal cell origin significantly altered the transcriptome of endometriotic organoids with over
235 4,500 DEG. These observations support the utility of a 3D organoid comprised of endometriotic
236 epithelium and stroma. Indeed, the genes expressed by EO largely mirrored those from
237 spontaneous endometriotic lesions in the baboon, and GSEA analyses confirmed coordinated
238 increases in TNFα signaling via NFKB, inflammatory responses, and hypoxia associated gene
239 sets. Analysis of organoid gene expression alterations associated with the origin of the stromal
240 cells identified several pathways known to be altered in endometriotic lesions, for example,
241 retinoic acid (RA) signaling, both the uptake of retinoid (*33*) and the production of retinoic acid
242 (RA) (*34*). Several enzymes in the RA pathway were altered in endometriotic organoids, including
243 decreased expression of *STRA6* and *CRABP2* (*35*), and increased *CYP26B1*. Telomerase
244 reverse transcriptase (*TERT*) expression was increased in ectopic organoids, as *TERT* was
245 amongst the most highly upregulated genes but was not altered in a comparison of stroma-only
246 organoids (Supplemental Fig 2). There is significant evidence for increased expression of *TERT*
247 in endometriosis in eutopic secretory endometrium (*36-40*) and endometriotic lesions (*41*). In
248 further support of the model, endometriotic lesions are progestin resistant (*42*) and, concordantly,
249 progesterone receptor expression was downregulated in EO. The expression of leukemia
250 inhibitory factor (*LIF*) was increased in EO, possibly due to local estrogenic activity (*43*) or
251 inflammatory signals (*44, 45*). These results demonstrate significant alignment of the EO
252 transcriptome with spontaneous disease and specific dysregulated pathways in endometriosis.

253 The immune system plays an important role in the establishment and progression of

254 endometriosis (*24, 46, 47*). Tissue resident immune cells are refluxed with menstrual tissue and
255 additional cells are recruited into the peritoneum where they interact with endometriotic lesions
256 (*48*). The pro-inflammatory cytokine *IL6* is common to all three coordinately increased hallmark
257 gene sets from EO and spontaneous endometriotic lesions from baboons (data not shown).
258 Interleukin-6 expression was increased in the spontaneous baboon lesions and EO and is
259 associated with chronic inflammation, endometriosis, and the presence of macrophages (*21, 48-*
260 *50*). IL-6 activates the expression of *CCL2* (also referred to as monocyte chemoattractant protein
261 1 or *MCP1*) in endothelial cells to recruit monocytes (*51*) and IL-6 is further produced by the
262 recruited macrophages and dendritic cells. Indeed, macrophages affect lesion establishment and
263 growth in a mouse model of endometriosis (*21, 47, 48*) and peritoneal macrophages from women
264 with endometriosis produce more IL-6 (*52*). Genes expressed in spontaneous lesions, but absent
265 from EO, were enriched in immune-related pathways indicating a role for immune cells in the
266 pathophysiology of endometriotic lesions that was absent in the model. Importantly, the invasive
267 capacity of EO was increased with the addition of proinflammatory macrophages, further
268 supporting this hypothesis. The mechanism by which the macrophages altered EO invasion is
269 undetermined, but IL-6 may be a key cytokine for the crosstalk between endometriotic lesions
270 and infiltrating macrophages. Our organoid model is an ideal system to uncover the crosstalk
271 between lesions and immune cells and is a subject for future studies.

272 Here we describe scaffold-free self-organized endometriotic organoids, comprised of both
273 endometriotic epithelial and stromal cells, combined with a novel model of attachment and
274 invasion of the peritoneum. Our findings support the idea that 3D culture systems allow for the
275 study of complex cell interactions and pathologically relevant processes like invasion and are a
276 promising new pre-clinical tool to evaluate therapeutic treatments for endometriosis. EO
277 recapitulated many of the transcriptomic features of spontaneous peritoneal endometriotic lesions
278 from the baboon and the model allowed for real-time imaging and quantification of organoid
279 invasion. The complexity of this model could be increased by altering conditions with exogenous
280 compounds or other cell types. Future studies utilizing this system can capitalize on this flexibility

281 with combinations of additional cell types, cell type genomic editing, and pharmacological
282 compounds. At present our *in vitro* model does not reflect the full complexities of macrophage
283 populations observed *in vivo* (*21, 47, 48*) and future experiments should investigate the interaction
284 of peripheral monocytes or naïve macrophages on EO and determine the effect on all cell types,
285 including the resultant macrophage phenotypes. Furthermore, EO could be integrated with
286 microfluidics cultures containing endometrium (*53, 54*) to study endometriosis associated
287 endometrial receptivity failure and decidualization defects.

288 In conclusion, our study suggests that EO recapitulate the characteristics of endometriotic
289 lesions and support the concept that organoids are an appropriate model for dissecting the
290 mechanisms that contribute to endometriotic lesion establishment.

291 **MATERIALS AND METHODS**

292 **Cell Lines**

293 Immortalized human endometriotic epithelial cells (12Z cells) (*16*) were cultured using
294 Dulbecco's modified Eagle's medium (DMEM)/F-12 (Gibco, USA) supplemented with 10%
295 Charcoal-dextran treated fetal bovine serum (CDS-FBS; Gibco, USA), 1X Pen/Strep (Gibco, USA)
296 and 1X sodium pyruvate (Gibco, USA)(*16, 55*). The human peritoneal mesothelial cell line LP9
297 was kindly provided by Dr. James G. Rheinwald (Harvard Medical School, Boston, MA, USA).
298 LP9 cells were maintained in a 1:1 ratio of M199 and Ham F12 media (Gibco), supplemented with
299 15% fetal bovine serum, 1% Penicillin/Streptomycin, 1% HEPES (Gibco), 1% GlutaMAX (Gibco),
300 10 ng/ml epidermal growth factor (EGF; Sigma, St Louis, MO, USA) and 400 ng/ml hydrocortisone
301 (Sigma). The immortalized human endometriotic stromal cell line (iEc-ESC) was established in
302 our laboratory (*17*). iEc-ESCs were cultured with phenol red–free DMEM/F12 medium
303 supplemented with 10% charcoal dextran stripped fetal bovine serum (CDS-FBS), 100 units/ml
304 of penicillin/streptomycin, and 1 mM sodium pyruvate. An immortalized human uterine fibroblast
305 cell line (iHUF) was established from the decidua parietalis from term placenta in our laboratory.
306 iHUF cells were cultured in phenol-red-free RPMI 1640 (Thermo Fisher Scientific) supplemented
307 with 10% CDS-FBS, 100 units/ml of penicillin/streptomycin, and 1 mM sodium pyruvate. THP1

308 cells (kindly provided by Dr. Margaret Petroff, Michigan State University) were grown in T75 flask
309 using RPMI1640 with 10% FBS in the presence of Antibiotic-Antimycotic in the suspension culture.
310 These cells were sub-cultured either in 6-well plates or T-25 flask and treated with 100nM (1:5000
311 µl of media) PMA (Phorbo 12-Myristate 13-Acetate, Cayman Chemicals, USA) to yield 60-70%
312 adherent cells at the end of 24 hours. The PMA exposure was repeated, and any floating non-
313 confluent cells were removed. The cell obtained following PMA treatment were designated as M0
314 macrophages and kept in pre-differentiated (M0) state for 2-4 days before exposing them to M1/
315 M2 differentiation. These M0 adherent macrophages were activated with 20 ng/ml IFN-gamma
316 (R&D Systems, USA) and 10pg/ ml of LPS (Sigma, USA.) for 24 hours to differentiate into M1
317 proinflammatory macrophages utilized to study effect of proinflammatory M1 macrophage on
318 endometriotic organoid culture system. All cell lines were maintained at 37ºC in an atmosphere
319 of 5% CO_2 in air.

320 RFP lentiviral vector (Ploc-RFP) was used to generate fluorescently tagged 12Z-RFP cell line.
321 EGFP lentiviral vector (pHX-EGFP) was utilized to generate LP9-GFP stable cell lines. iEC-ESCs
322 and iHUF cells were tagged with Azurite blue using pLV-Azurite (Addgene plasmid 36086).
323 Lentiviral transductions were performed according to manufacturers' protocols and successfully
324 tagged cells were further sorted on a Beckman Coulter MoFlow Astrios (Indianapolis, IN, USA).

325 **Generation of Endometriotic Organoids**

326 12Z and stromal cells were trypsinized in the flask and cell suspensions were centrifuged at 200
327 x*g* for 5 minutes. Both epithelial and stromal cell pellets were then suspended in complete
328 MammoCult human medium (STEMCELL Technologies, Inc., 05620) supplemented with
329 hydrocortisone and heparin as per the manufacturer's instructions and 1% pen/strep (Sigma,
330 P0781) to similar densities. Epithelial and stromal cells were mixed at a 1:50 ratio by volume and
331 50uL of epithelial-stromal cell suspension was seeded into 1.5% (w/v) agarose 3D micro-molded
332 plate, prepared according to the manufacturer's instructions (MicroTissues® 3D Petri Dish®
333 micro-mold spheroids, Sigma, Z764043). Media was changed every 2-3 days. 12Z+iHUF
334 organoids were used as a control, since a normal epithelial cell line of endometrial origin is not

335 currently available.

336 **Organoid Invasion Model**

337 To mimic the structure of the peritoneum, an ice cold LP9 cell suspension was mixed with ice
338 cold Matrigel (Corning, 536232) at a ratio of 2:1(v:v), 30ul drops of Matrigel-cell suspension were
339 plated into 96-well plate, at a density of 2-2.5x10^4 cells per well, allowed to set at 37℃ for 3-4
340 hours until solidified and overlaid with 100ul MammoCult growth medium. The next day, the day
341 4 endometriotic organoids were harvested from 3D Petri Dishes® by pipetting and then seeded
342 on to the top of Matrigel-LP9-GFP layer in 96-well plates in 100ul MammoCult growth medium.
343 Organoid invasion into the LP9-GFP/Matrigel layer were imaged every 48 hours using confocal
344 microscopy.

345 **Organoid Imaging**

346 Organoids were imaged using a Nikon Eclipse Ti inverted microscope using a Nikon C2 +
347 confocal microscope laser scanner. For each organoid, z-stacks were generated with a 10μm
348 increment, and tiled scans were set up to image the entire width and depth of the organoid with
349 10x air objective. The position of the each organoid was recorded as x,y coordinate by ND
350 Acquisition of NIS-Elements software. For organoid sections, z-stacks were generated with 0.5μm
351 increment using 40X oil objective. Images were merged using NIS-Elements C2 version 4.13.

352 **Quantification of Invasion**

353 Commercial software Imaris x64 7.4.2 (Bitplane) was used for image analysis. In order to
354 quantify the invasion of the organoid stromal cells into the peritoneal mesothelial cells, 3D surface
355 models of the LP9-GFP cell layer, and the stromal cells-Azurite blue were created. Using the
356 measurement function in Imaris, and using orthogonal slicers in XY, YZ and ZX planes, the linear
357 distance between the organoid tip and the organoid migrating front on to the peritoneal cells were
358 calculated. The distances were calculated at different time points in order to calculate velocity of
359 organoid movement as a function of time. Seven to ten organoids for each time point in different
360 groups were evaluated to account for heterogeneity in organoid structure as well as movement.

361 **Immunofluorescence Staining**

362 Agarose 3D Petri Dishes® containing organoids were removed from the tissue culture plate
363 and the medium inside was removed gently by pipetting under a dissecting microscope.
364 Organoids were sealed within the agarose dish with lukewarm 1.5% (w/v) agarose in 1×PBS. The
365 sealed 3D Petri Dishes® containing organoids were then fixed in 4% paraformaldehyde in 1×PBS
366 at 4°C overnight, rinsed briefly in 1×PBS, stored in 70% EtOH and processed for standard paraffin
367 embedding and sectioning at 6μm. Organoid sections were dewaxed, and then rehydrated with a
368 graded alcohol series, followed by heat-mediated antigen retrieval in citrate buffer (Vector
369 Laboratories, H3300) and then hydrogen peroxide treatment. Sections were blocked for 1 h in 10%
370 normal horse serum (Vector Laboratories, S-2000) in PBS and incubated overnight at 4°C in
371 primary antibodies. Organoid sections were incubated in respective species specific
372 fluorochrome-conjugated secondary antibodies following an overnight incubation with the primary
373 antibodies. Slides were then mounted with Antifade Mounting Medium with DAPI (Vector
374 Laboratories, H-1200). Images were captured with a Nikon Eclipse Ti inverted microscope using
375 software from NIS Elements, Inc. (Nikon, Melville, NY). The primary antibodies used were
376 Vimentin polyclonal antibody (5741S) from Cell Signaling Technology, Inc. (Waltham, MA).
377 Cytokeratin, pan (mixture) monoclonal antibody (C2562), from Sigma-Aldrich (St. Louis, MO). The
378 secondary antibodies were: DyLight 594 goat anti-rabbit IgG antibody (DI-1594) from Vector
379 Laboratories (Burlingame, CA). Alexa Fluor® 488 AffiniPure donkey anti-mouse IgG (715-545-
380 150) from Jackson ImmunoResearch Laboratories Inc. (West Grove, PA).

381 **RNA-sequencing and Data Analysis**

382 For RNA-sequencing, the Arcturus PicoPure RNA Isolation Kit (Themo Fisher Scientific,
383 12204-01), including an on-column DNA digestion using the RNAse-free DNAse set (Qiagen;
384 79254), was used to purify RNA from whole organoids. Total RNA was isolated from snap-frozen
385 tissues homogenized in TRIzol reagent (Thermo Fisher; 15596018) following the manufacturer's
386 instructions. RNA was stored at -80°C in nuclease-free water and concentration was determined
387 with a Nanodrop 1000 instrument (Thermo Fisher Scientific). Samples were sent to a sequencing
388 facility (Novogene Corporation Inc., Chula Vista, CA) for RNA integrity analysis, library preparation,

389 and sequencing. Libraries were prepared with an TruSeq mRNA kit (Illumina Inc., San Diego, CA)
390 and sequenced (paired end 150 bp) on a NovaSeq 6000 instrument (Illumina Inc.) to an average
391 depth of 39 million fragments per sample. Reads were quality trimmed and adapters were
392 removed using TrimGalore (version 0.6.5) (*56*), and quality trimmed reads were assessed with
393 FastQC (version 0.11.7). Trimmed reads were mapped to *Homo sapiens* genome assembly
394 GRCh38 (hg38) or *Papio anubis* (version 3.0) using using HISAT2 (version 2.0.3) (*57*). Reads
395 overlapping Ensembl annotations (version 99) (*58*) were quantified with featureCounts (version
396 1.6.2) (*59*) prior to model-based differential expression (DE) analysis using the edgeR-robust
397 method (version 4.0.3) (*60*) in R. Genes with low counts per million (CPM) were removed using
398 the filterByExpr function from edgeR. Transcriptome-wide read distributions were plotted to
399 ensure a similar distribution across all samples with boxplots of log-transformed CPM values.
400 Multidimensional scaling plots, generated with the plotMDS function of edgeR, were used to verify
401 group separation prior to statistical analysis. Principal component analysis of normalized counts
402 was conducted with the prcomp function in R using the top 500 variable genes. Differentially
403 expressed genes (DEG) were identified as false discovery rate (FDR) p-value less than 0.05.
404 The hclust package was used for hierarchical clustering (ward.D) of Euclidean distances.
405 Heat maps were generated using log-transformed transcript per million values (TPM) in pheatmap
406 (version 1.0.12). Where necessary, baboon Ensembl genes were converted to human entrez
407 identifiers with the human ortholog table downloaded from Biomart (version 101). The phyper
408 function in R was used for hypergeometric tests of overlapping genes. Gene set enrichment and
409 over-representation analyses were completed with clusterProfiler package (version 3.16.1) using
410 mSigDB and KEGG reference databases.

411 **Statistical Analysis**

412 Unless otherwise stated, statistical analysis was performed using GraphPad Prism 9.00
413 (GraphPad). All data were expressed as mean ± SD. The student's t test was used for
414 comparisons between the 2 groups, and 1-way ANOVA with a post hoc test least-significant
415 difference was used for multiple comparisons. $P < 0.05$ was considered statistically significant (2-

416 tailed).

417 **LIST OF SUPPLEMENTARY MATERIALS**

418 Fig. S1. Epithelial and stromal cell organization in organoid culture.

419 Fig. S2. Telomerase reverse transcriptase (TERT) expression in organoids.

420 Fig. S3. Macrophages present in baboon endometriotic lesions.

421 Movie S1. Endometriotic organoids self-organize into epithelium and stromal compartments.

422 Movie S2. Confocal live imaging of EO invasion through a mesothelial cell layer over 8 days.

423 **REFERENCES**

424 1. L. C. Giudice, Clinical practice. Endometriosis. *N Engl J Med* **362**, 2389-2398 (2010).
425 2. Practice Committee of the American Society for Reproductive Medicine. Treatment of pelvic
426 pain associated with endometriosis. *Fertil Steril* **90**, S260-269 (2008).
427 3. Endometriosis and infertility: a committee opinion. *Fertil Steril* **98**, 591-598 (2012).
428 4. R. O. Burney, L. C. Giudice, Pathogenesis and pathophysiology of endometriosis. *Fertil Steril*
429 **98**, 511-519 (2012).
430 5. H. L. Yang, W. J. Zhou, K. K. Chang, J. Mei, L. Q. Huang, M. Y. Wang, Y. Meng, S. Y. Ha, D.
431 J. Li, M. Q. Li, The crosstalk between endometrial stromal cells and macrophages impairs
432 cytotoxicity of NK cells in endometriosis by secreting IL-10 and TGF-β. *Reproduction* **154**,
433 815-825 (2017).
434 6. A. T. Fazleabas, A baboon model for inducing endometriosis. *Methods Mol Med* **121**, 95-99
435 (2006).
436 7. P. Harirchian, I. Gashaw, S. T. Lipskind, A. G. Braundmeier, J. M. Hastings, M. R. Olson, A. T.
437 Fazleabas, Lesion kinetics in a non-human primate model of endometriosis. *Hum Reprod* **27**,
438 2341-2351 (2012).
439 8. K. L. Bruner-Tran, S. Mokshagundam, J. L. Herington, T. Ding, K. G. Osteen, Rodent Models
440 of Experimental Endometriosis: Identifying Mechanisms of Disease and Therapeutic Targets.
441 *Curr Womens Health Rev* **14**, 173-188 (2018).
442 9. F. Schutgens, M. C. Verhaar, M. B. Rookmaaker, Pluripotent stem cell-derived kidney
443 organoids: An in vivo-like in vitro technology. *Eur J Pharmacol* **790**, 12-20 (2016).
444 10. S. L. Leibel, R. N. McVicar, A. M. Winquist, W. D. Niles, E. Y. Snyder, Generation of Complete
445 Multi-Cell Type Lung Organoids From Human Embryonic and Patient-Specific Induced
446 Pluripotent Stem Cells for Infectious Disease Modeling and Therapeutics Validation. *Curr*
447 *Protoc Stem Cell Biol* **54**, e118 (2020).
448 11. M. Boretto, B. Cox, M. Noben, N. Hendriks, A. Fassbender, H. Roose, F. Amant, D.
449 Timmerman, C. Tomassetti, A. Vanhie, C. Meuleman, M. Ferrante, H. Vankelecom,
450 Development of organoids from mouse and human endometrium showing endometrial
451 epithelium physiology and long-term expandability. *Development* **144**, 1775-1786 (2017).
452 12. M. Y. Turco, L. Gardner, J. Hughes, T. Cindrova-Davies, M. J. Gomez, L. Farrell, M.
453 Hollinshead, S. G. E. Marsh, J. J. Brosens, H. O. Critchley, B. D. Simons, M. Hemberger, B.
454 K. Koo, A. Moffett, G. J. Burton, Long-term, hormone-responsive organoid cultures of human
455 endometrium in a chemically defined medium. *Nat Cell Biol* **19**, 568-577 (2017).
456 13. T. Wiwatpanit, A. R. Murphy, Z. Lu, M. Urbanek, J. E. Burdette, T. K. Woodruff, J. J. Kim,
457 Scaffold-Free Endometrial Organoids Respond to Excess Androgens Associated With
458 Polycystic Ovarian Syndrome. *J Clin Endocrinol Metab* **105**, (2020).
459 14. M. Boretto, N. Maenhoudt, X. Luo, A. Hennes, B. Boeckx, B. Bui, R. Heremans, L. Perneel,
460 H. Kobayashi, I. Van Zundert, H. Brems, B. Cox, M. Ferrante, I. H. Uji, K. P. Koh, T. D'Hooghe,
461 A. Vanhie, I. Vergote, C. Meuleman, C. Tomassetti, D. Lambrechts, J. Vriens, D. Timmerman,
462 H. Vankelecom, Patient-derived organoids from endometrial disease capture clinical

463 heterogeneity and are amenable to drug screening. *Nat Cell Biol* **21**, 1041-1051 (2019).
464 15. T. M. Rawlings, K. Makwana, D. M. Taylor, M. A. Molè, K. J. Fishwick, M. Tryfonos, J. Odendaal,
465 A. Hawkes, M. Zernicka-Goetz, G. M. Hartshorne, J. J. Brosens, E. S. Lucas, Modelling the
466 impact of decidual senescence on embryo implantation in human endometrial assembloids.
467 *Elife* **10**, (2021).
468 16. A. Zeitvogel, R. Baumann, A. Starzinski-Powitz, Identification of an invasive, N-cadherin-
469 expressing epithelial cell type in endometriosis using a new cell culture model. *Am J Pathol*
470 **159**, 1839-1852 (2001).
471 17. Y. Song, N. R. Joshi, E. Vegter, S. Hrbek, B. A. Lessey, A. T. Fazleabas, Establishment of an
472 Immortalized Endometriotic Stromal Cell Line from Human Ovarian Endometrioma.
473 *Reproductive sciences (Thousand Oaks, Calif.)*, (2020).
474 18. W. Xiong, L. Zhang, L. Yu, W. Xie, Y. Man, Y. Xiong, H. Liu, Y. Liu, Estradiol promotes cells
475 invasion by activating β-catenin signaling pathway in endometriosis. *Reproduction* **150**, 507-
476 516 (2015).
477 19. Y. Du, Z. Zhang, W. Xiong, N. Li, H. Liu, H. He, Q. Li, Y. Liu, L. Zhang, Estradiol promotes
478 EMT in endometriosis via MALAT1/miR200s sponge function. *Reproduction* **157**, 179-188
479 (2019).
480 20. S. H. Ahn, S. P. Monsanto, C. Miller, S. S. Singh, R. Thomas, C. Tayade, Pathophysiology and
481 Immune Dysfunction in Endometriosis. *Biomed Res Int* **2015**, 795976 (2015).
482 21. M. Bacci, A. Capobianco, A. Monno, L. Cottone, F. Di Puppo, B. Camisa, M. Mariani, C.
483 Brignole, M. Ponzoni, S. Ferrari, P. Panina-Bordignon, A. A. Manfredi, P. Rovere-Querini,
484 Macrophages are alternatively activated in patients with endometriosis and required for
485 growth and vascularization of lesions in a mouse model of disease. *Am J Pathol* **175**, 547-
486 556 (2009).
487 22. E. Haber, H. D. Danenberg, N. Koroukhov, R. Ron-El, G. Golomb, M. Schachter, Peritoneal
488 macrophage depletion by liposomal bisphosphonate attenuates endometriosis in the rat
489 model. *Hum Reprod* **24**, 398-407 (2009).
490 23. P. Vercellini, P. Vigano, E. Somigliana, L. Fedele, Endometriosis: pathogenesis and treatment.
491 *Nat Rev Endocrinol* **10**, 261-275 (2014).
492 24. G. Izumi, K. Koga, M. Takamura, T. Makabe, E. Satake, A. Takeuchi, A. Taguchi, Y. Urata, T.
493 Fujii, Y. Osuga, Involvement of immune cells in the pathogenesis of endometriosis. *J Obstet*
494 *Gynaecol Res* **44**, 191-198 (2018).
495 25. J. A. Sampson, Peritoneal endometriosis due to the menstrual dissemination of endometrial
496 tissue into the peritoneal cavity. *American Journal of Obstetrics & Gynecology* **14**, 422-469
497 (1927).
498 26. K. T. Zondervan, C. M. Becker, K. Koga, S. A. Missmer, R. N. Taylor, P. Vigano, Endometriosis.
499 *Nat Rev Dis Primers* **4**, 9 (2018).
500 27. J. R. H. Wendel, X. Wang, L. J. Smith, S. M. Hawkins, Three-Dimensional Biofabrication
501 Models of Endometriosis and the Endometriotic Microenvironment. *Biomedicines* **8**, (2020).
502 28. A. Stejskalova, V. Fincke, M. Nowak, Y. Schmidt, K. Borrmann, M. K. von Wahlde, S. D.
503 Schafer, L. Kiesel, B. Greve, M. Gotte, Collagen I triggers directional migration, invasion and

matrix remodeling of stroma cells in a 3D spheroid model of endometriosis. *Sci Rep* **11**, 4115 (2021).

29. Y. Park, J. G. Jung, Z. C. Yu, R. Asaka, W. Shen, Y. Wang, W. H. Jung, A. Tomaszewski, G. Shimberg, Y. Chen, V. Parimi, S. Gaillard, I. M. Shih, T. L. Wang, A novel human endometrial epithelial cell line for modeling gynecological diseases and for drug screening. *Lab Invest* **101**, 1505-1512 (2021).
30. C. A. Witz, I. A. Monotoya-Rodriguez, R. S. Schenken, Whole explants of peritoneum and endometrium: a novel model of the early endometriosis lesion. *Fertil Steril* **71**, 56-60 (1999).
31. M. Nisolle, F. Casanas-Roux, J. Donnez, Early-stage endometriosis: adhesion and growth of human menstrual endometrium in nude mice. *Fertil Steril* **74**, 306-312 (2000).
32. L. L. Lin, S. Makwana, M. Chen, C. M. Wang, L. H. Gillette, T. H. Huang, R. O. Burney, B. J. Nicholson, N. B. Kirma, Cellular junction and mesenchymal factors delineate an endometriosis-specific response of endometrial stromal cells to the mesothelium. *Mol Cell Endocrinol* **539**, 111481 (2021).
33. M. E. Pavone, S. Reierstad, H. Sun, M. Milad, S. E. Bulun, Y. H. Cheng, Altered retinoid uptake and action contributes to cell survival in endometriosis. *J Clin Endocrinol Metab* **95**, E300-309 (2010).
34. K. Pierzchalski, R. N. Taylor, C. Nezhat, J. W. Jones, J. L. Napoli, G. Yang, M. A. Kane, N. Sidell, Retinoic acid biosynthesis is impaired in human and murine endometriosis. *Biol Reprod* **91**, 84 (2014).
35. M. E. Pavone, A. R. Grover, R. Confino, E. K. Pearson, S. Malpani, Y.-H. Cheng, A. Fazleabas, S. Bulun, Retinoic acid action is altered within endometrium of baboons affected with endometriosis. *Journal of Endometriosis and Pelvic Pain Disorders*, (2022).
36. C. M. Kim, Y. J. Oh, S. H. Cho, D. J. Chung, J. Y. Hwang, K. H. Park, D. J. Cho, Y. M. Choi, B. S. Lee, Increased telomerase activity and human telomerase reverse transcriptase mRNA expression in the endometrium of patients with endometriosis. *Hum Reprod* **22**, 843-849 (2007).
37. D. K. Hapangama, M. A. Turner, J. A. Drury, S. Quenby, G. Saretzki, C. Martin-Ruiz, T. Von Zglinicki, Endometriosis is associated with aberrant endometrial expression of telomerase and increased telomere length. *Hum Reprod* **23**, 1511-1519 (2008).
38. A. J. Valentijn, K. Palial, H. Al-Lamee, N. Tempest, J. Drury, T. Von Zglinicki, G. Saretzki, P. Murray, C. E. Gargett, D. K. Hapangama, SSEA-1 isolates human endometrial basal glandular epithelial cells: phenotypic and functional characterization and implications in the pathogenesis of endometriosis. *Hum Reprod* **28**, 2695-2708 (2013).
39. F. A. Mafra, D. M. Christofolini, V. Cavalcanti, F. L. Vilarino, G. M. André, P. Kato, B. Bianco, C. P. Barbosa, Aberrant telomerase expression in the endometrium of infertile women with deep endometriosis. *Arch Med Res* **45**, 31-35 (2014).
40. D. K. Hapangama, A. Kamal, G. Saretzki, Implications of telomeres and telomerase in endometrial pathology. *Hum Reprod Update* **23**, 166-187 (2017).
41. D. K. Hapangama, M. A. Turner, J. Drury, L. Heathcote, Y. Afshar, P. A. Mavrogianis, A. T. Fazleabas, Aberrant expression of regulators of cell-fate found in eutopic endometrium is

545 found in matched ectopic endometrium among women and in a baboon model of
546 endometriosis. *Hum Reprod* **25**, 2840-2850 (2010).
547 42. G. R. Attia, K. Zeitoun, D. Edwards, A. Johns, B. R. Carr, S. E. Bulun, Progesterone receptor
548 isoform A but not B is expressed in endometriosis. *J Clin Endocrinol Metab* **85**, 2897-2902
549 (2000).
550 43. S. E. Bulun, S. Yang, Z. Fang, B. Gurates, M. Tamura, S. Sebastian, Estrogen production and
551 metabolism in endometriosis. *Annals of the New York Academy of Sciences* **955**, 75-85;
552 discussion 86-78, 396-406 (2002).
553 44. D. Knight, Leukaemia inhibitory factor (LIF): a cytokine of emerging importance in chronic
554 airway inflammation. *Pulm Pharmacol Ther* **14**, 169-176 (2001).
555 45. G. X. Rosario, C. L. Stewart, The Multifaceted Actions of Leukaemia Inhibitory Factor in
556 Mediating Uterine Receptivity and Embryo Implantation. *Am J Reprod Immunol* **75**, 246-255
557 (2016).
558 46. D. I. Lebovic, M. D. Mueller, R. N. Taylor, Immunobiology of endometriosis. *Fertil Steril* **75**, 1-
559 10 (2001).
560 47. C. Hogg, A. W. Horne, E. Greaves, Endometriosis-Associated Macrophages: Origin,
561 Phenotype, and Function. *Front Endocrinol (Lausanne)* **11**, 7 (2020).
562 48. C. Hogg, K. Panir, P. Dhami, M. Rosser, M. Mack, D. Soong, J. W. Pollard, S. J. Jenkins, A.
563 W. Horne, E. Greaves, Macrophages inhibit and enhance endometriosis depending on their
564 origin. *Proc Natl Acad Sci U S A* **118**, (2021).
565 49. C. Gabay, Interleukin-6 and chronic inflammation. *Arthritis Res Ther* **8 Suppl 2**, S3 (2006).
566 50. A. Capobianco, A. Monno, L. Cottone, M. A. Venneri, D. Biziato, F. Di Puppo, S. Ferrari, M.
567 De Palma, A. A. Manfredi, P. Rovere-Querini, Proangiogenic Tie2(+) macrophages infiltrate
568 human and murine endometriotic lesions and dictate their growth in a mouse model of the
569 disease. *Am J Pathol* **179**, 2651-2659 (2011).
570 51. M. Romano, M. Sironi, C. Toniatti, N. Polentarutti, P. Fruscella, P. Ghezzi, R. Faggioni, W.
571 Luini, V. van Hinsbergh, S. Sozzani, F. Bussolino, V. Poli, G. Ciliberto, A. Mantovani, Role of
572 IL-6 and its soluble receptor in induction of chemokines and leukocyte recruitment. *Immunity*
573 **6**, 315-325 (1997).
574 52. P. Montagna, S. Capellino, B. Villaggio, V. Remorgida, N. Ragni, M. Cutolo, S. Ferrero,
575 Peritoneal fluid macrophages in endometriosis: correlation between the expression of
576 estrogen receptors and inflammation. *Fertil Steril* **90**, 156-164 (2008).
577 53. H. Campo, A. Murphy, S. Yildiz, T. Woodruff, I. Cervelló, J. J. Kim, Microphysiological Modeling
578 of the Human Endometrium. *Tissue Eng Part A* **26**, 759-768 (2020).
579 54. S. Xiao, J. R. Coppeta, H. B. Rogers, B. C. Isenberg, J. Zhu, S. A. Olalekan, K. E. McKinnon,
580 D. Dokic, A. S. Rashedi, D. J. Haisenleder, S. S. Malpani, C. A. Arnold-Murray, K. Chen, M.
581 Jiang, L. Bai, C. T. Nguyen, J. Zhang, M. M. Laronda, T. J. Hope, K. P. Maniar, M. E. Pavone,
582 M. J. Avram, E. C. Sefton, S. Getsios, J. E. Burdette, J. J. Kim, J. T. Borenstein, T. K. Woodruff,
583 A microfluidic culture model of the human reproductive tract and 28-day menstrual cycle. *Nat*
584 *Commun* **8**, 14584 (2017).
585 55. S. K. Banu, J. Lee, A. Starzinski-Powitz, J. A. Arosh, Gene expression profiles and functional

586 characterization of human immortalized endometriotic epithelial and stromal cells. *Fertil Steril*
587 **90**, 972-987 (2008).
588 56. M. Martin, Cutadapt removes adapter sequences from high-throughput sequencing reads.
589 *EMBnet.journal* **17**, pp-10 (2011).
590 57. D. Kim, B. Langmead, S. L. Salzberg, HISAT: A fast spliced aligner with low memory
591 requirements. *Nat Methods* **12**, 357-360 (2015).
592 58. B. L. Aken, S. Ayling, D. Barrell, L. Clarke, V. Curwen, S. Fairley, J. Fernandez Banet, K. Billis,
593 C. Garcia Giron, T. Hourlier, K. Howe, A. Kahari, F. Kokocinski, F. J. Martin, D. N. Murphy, R.
594 Nag, M. Ruffier, M. Schuster, Y. A. Tang, J. H. Vogel, S. White, A. Zadissa, P. Flicek, S. M.
595 Searle, The Ensembl gene annotation system. *Database (Oxford)* **2016**, 1-19 (2016).
596 59. Y. Liao, G. K. Smyth, W. Shi, featureCounts: an efficient general purpose program for
597 assigning sequence reads to genomic features. *Bioinformatics* **30**, 923-930 (2014).
598 60. X. Zhou, H. Lindsay, M. D. Robinson, Robustly detecting differential expression in RNA
599 sequencing data using observation weights. *Nucleic Acids Res* **42**, e91 (2014).
600

ACKNOWLEDGEMENTS

The authors would like to sincerely thank all members of the Fazleabas laboratory, particularly Samantha Hrbek, Erin Vegter, and Ariadna Ochoa-Bernal, for their contributions to this project. We also thank Stephanie Celano for her assistance with live-cell imaging.

FUNDING

National Institutes of Health grant R01HD083273 (ATF)
National Institutes of Health grant R01HD099090 (ATF)
National Institutes of Health grant F32HD104478 (GWB)
Endometriosis Foundation of America (ATF)

AUTHOR CONTRIBUTIONS

Conceptualization: YS, GWB, ATF
Methodology: RA, JK
Investigation: YS, GWB, NRJ, RA
Visualization: YS, RA
Funding acquisition: GB, ATF
Project administration: ATF
Writing – original draft: YS, GB
Writing – review & editing: YS, GB, ATF, RA, JK

COMPETING INTERESTS

Authors declare that they have no competing interests.

DATA AND MATERIALS AVAILABILITY

Raw FASTQ files were deposited in the NCBI Gene Expression Omnibus (GSE######).

628 **FIGURES**

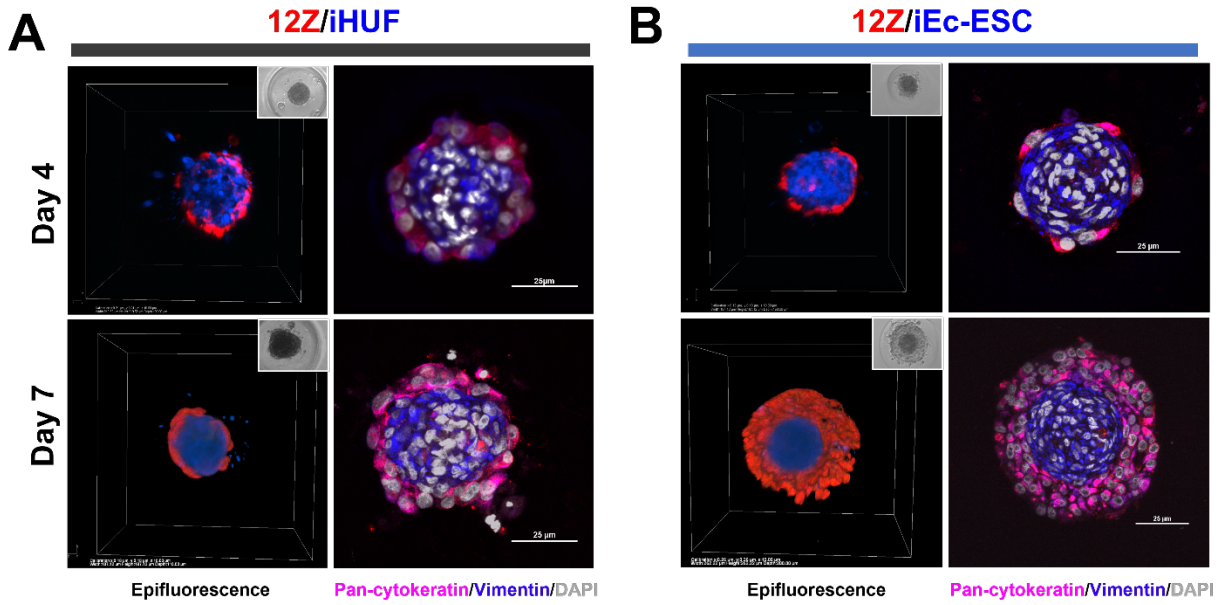

629

630

631 **Fig 1. Organoid structure.** Time course of organoid development derived from (A) 12Z-
632 RFP/iHUF-Azurite Blue and (B) 12Z-RFP/iEc-ESC-Azurite Blue (endometriotic organoids,
633 EO). The left panels are 3D views and inserts are phase contrast images. The right panels
634 are immunofluorescent staining of vimentin (blue) and pan-cytokeratin (red). Scale bar =
635 25 μm.

636

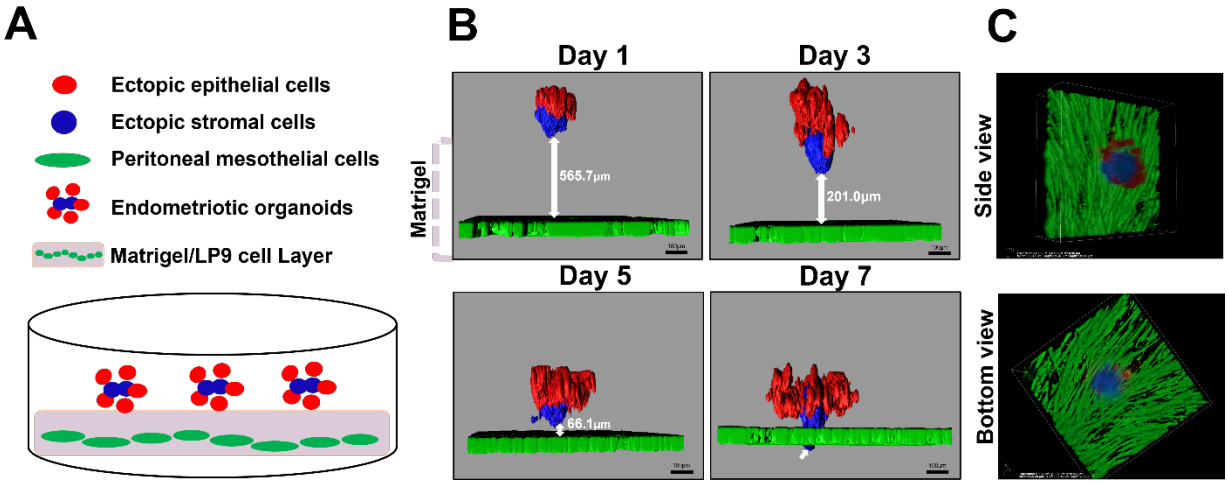

Fig 2. Organoid invasion model. Endometriotic organoids invade a 3D model of the peritoneum. (A) Schematic of the organoid invasion model. (B) Time course of organoid invasion quantified with Imaris image analysis software and relative to invasion into the mesothelial cell layer. Ectopic stromal cells were the leading edge of invasion through the LP9 cells. Note the penetration of organoids through the extracellular matrix and mesothelial cell layer in a time dependent manner. (C) Representative side view and bottom view of an EO invading the LP9 cells with stromal cells at the leading edge.

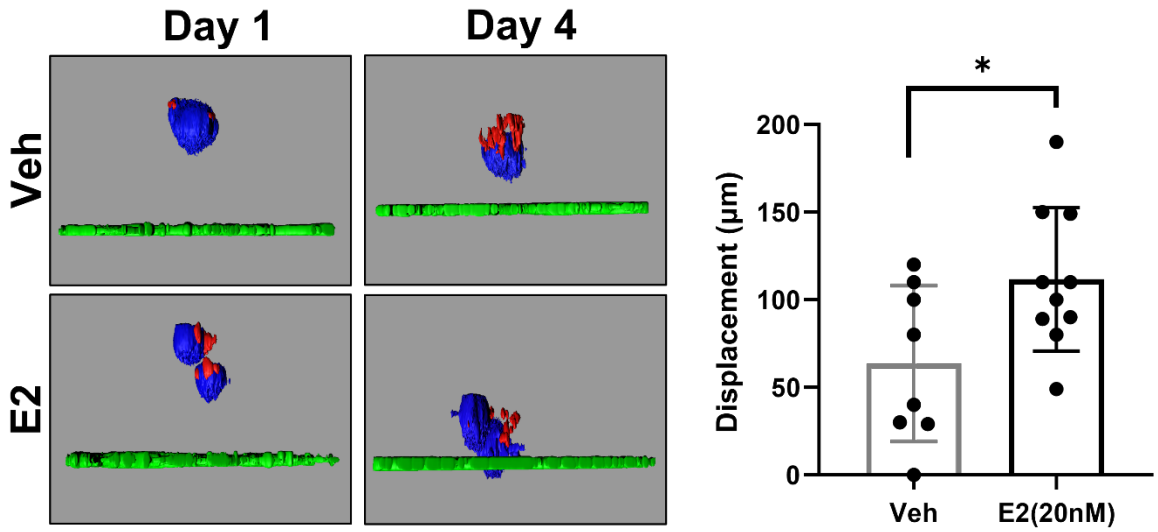

647

648

649 **Fig 3. Estrogen stimulates invasion of endometriotic organoids (EO).** Day 4 EO were
650 seeded on an LP9/Matrigel layer and treated with vehicle (ethanol, n=8) or estradiol (E2,
651 20nM, n=10) for 4 days. The EO were imaged on days 1 and 4 using fluorescent confocal
652 microscopy and invasion, relative to the LP9 cell layer was quantified. Invasion was
653 increased by 1.8-fold in the presence of E2. *P<0.05

654

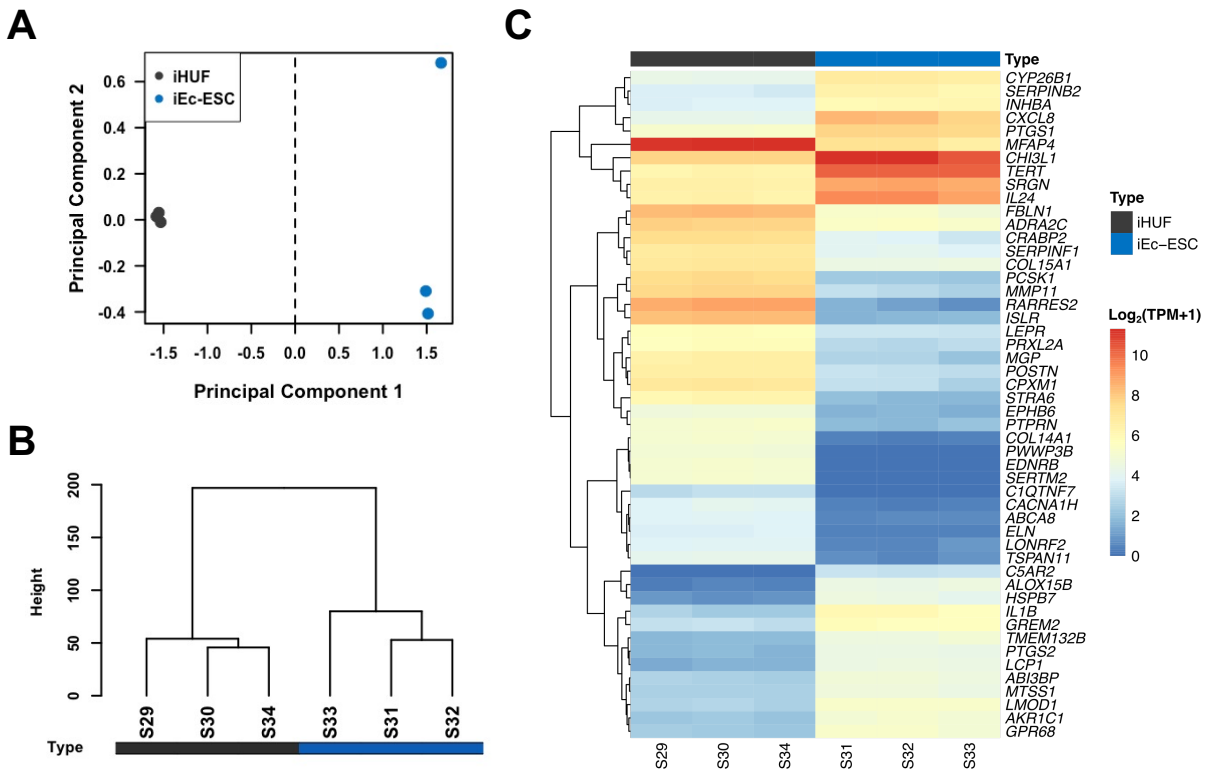

Fig 4. Stromal cell origin alters organoid gene expression. (A) Principal component plot demonstrating transcriptome separation between iEc-ESC/12Z (EO) and iHUF/12Z organoids. (B) Unsupervised hierarchical clustering dendrogram confirming separation of sample groups and (C) a heat map of the top 50 differentially expressed genes with hierarchical gene clustering.

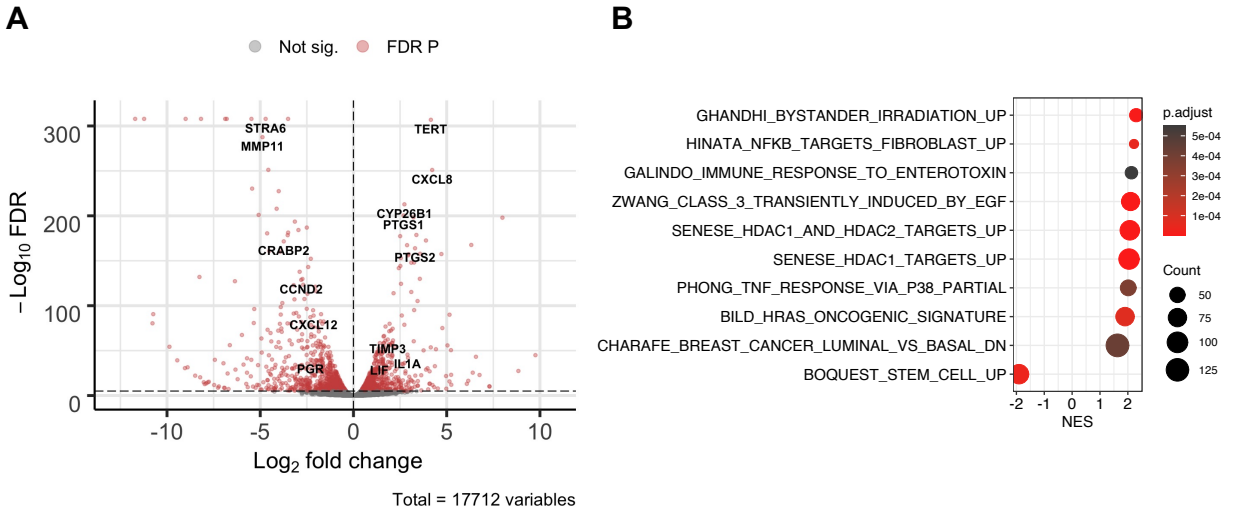

Fig 5. Transcriptome alterations in EO versus iHUF/12Z organoids. (A) Volcano plot highlighting several top downregulated and upregulated genes in EO. (B) The top MSigDB C2 enriched gene sets from human organoids. A positive normalized enrichment score (NES) indicates activation, or increased expression, of the gene set in EO.

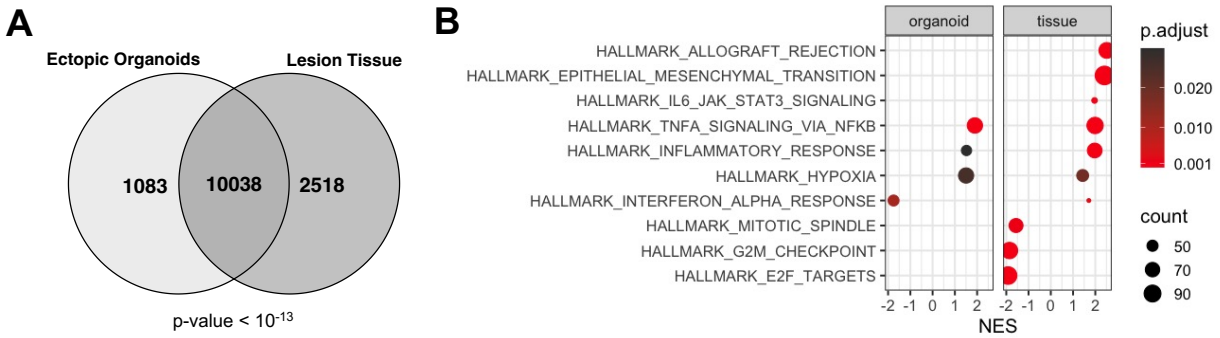

Fig 6. Endometriotic organoids (EO) and baboon lesion gene expression signatures are similar. (A) The overlap of all expressed genes in EO and baboon lesions from spontaneous endometriosis is highly significant. (B) Gene set enrichment analyses showed similar enrichment of NFKB, inflammatory response and hypoxia genes. NES= normalized enrichment score

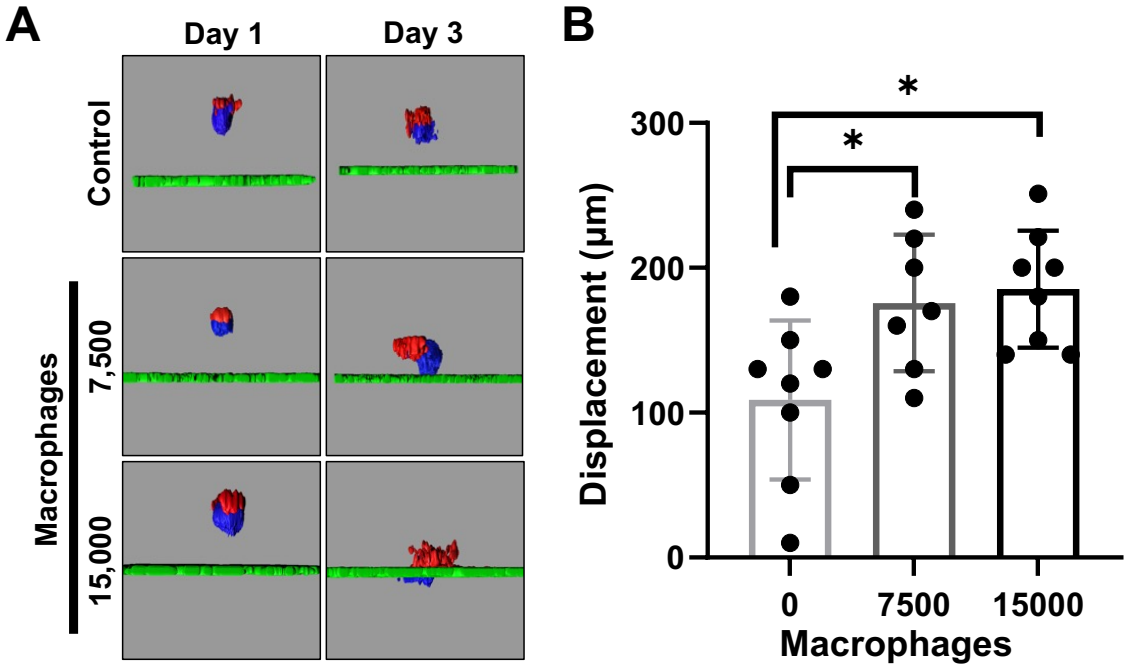

Fig 7. Proinflammatory macrophages increase EO invasion. (A) Day 4 EO were seeded on an LP9/Matrigel layer and M1 macrophages (7,500 or 15,000) were added to the plates after 3h. The EO were imaged on days 1 and 3 using fluorescent confocal microscopy and (B) invasion relative to the LP9 cell layer, was quantified. Invasion of EO was increased in co-culture with 7,500 or 15,000 macrophages by 1.6- or 1.7-fold, respectively. Control n=8; M1 7,500 n=7; M1 15,000 n=8 *P<0.05

686 **Table 1. Enrichment for immune-related genes in spontaneous endometriotic lesions.** Top 10 enriched biological
687 process gene ontology terms from genes expressed in baboon lesions and not human organoids.
688

PANTHER GO Slim (BP)	REFLIST	Input	Expected	Direction	Fold Enrichment	p-value	FDR
immune system process (GO:0002376)	258	128	44.67	+	2.87	3.56E-20	7.74E-18
immune response (GO:0006955)	163	90	28.22	+	3.19	9.35E-17	1.13E-14
cell surface receptor signaling pathway (GO:0007166)	544	177	94.18	+	1.88	1.44E-12	1.49E-10
signaling (GO:0023052)	1208	321	209.14	+	1.53	2.95E-12	2.92E-10
cell communication (GO:0007154)	1219	320	211.05	+	1.52	1.29E-11	1.08E-09
multicellular organismal process (GO:0032501)	682	204	118.08	+	1.73	1.45E-11	1.17E-09
signal transduction (GO:0007165)	1136	298	196.68	+	1.52	7.61E-11	4.73E-09
regulation of immune system process (GO:0002682)	127	64	21.99	+	2.91	7.87E-11	4.75E-09
leukocyte activation (GO:0045321)	57	40	9.87	+	4.05	2.04E-10	1.11E-08
positive regulation of immune system process (GO:0002684)	87	50	15.06	+	3.32	2.25E-10	1.19E-08

689